Economic Geology
Vol. 87, 1992, pp. 1813–1829

Reaction of Some Trioctahedral Micas with Copper Sulfate Solutions at 25°C and 1 Atmosphere: An Electron Microprobe and Transmission Electron Microscopy Investigation

EUGENE S. ILTON,

Department of Earth and Environmental Sciences, Williams Hall 31, Lehigh University, Bethlehem, Pennsylvania 18015-3188

DRUMMOND EARLEY III, DIANNE MAROZAS,

U. S. Bureau of Mines, 5629 Minnehaha Avenue South, Minneapolis, Minnesota 55417

AND DAVID R. VEBLEN

Department of Earth and Planetary Sciences, Johns Hopkins University, Baltimore, Maryland 21218

Abstract

Reaction of biotite and phlogopite with acidic, $CuSO_4$-rich aqueous solutions at 25° ± 3°C and 1 atm, produced submicroscopic inclusions of a copper-rich, sulfur-absent phase, identified by electron diffraction and analytical electron microscopy as native copper. The copper inclusions lie in the interlayer region of the mica and are associated with copper-enriched, expanded (hydrated) interlayers and potassium depletion. The inclusions, and associated biotite textures and compositions produced in the experiments, are similar to those documented in naturally occurring biotites from rocks associated with porphyry copper deposits (Ilton and Veblen, 1988). The experiments support the suggestion of Ilton and Veblen (1990, 1992) that this mode of copper enrichment in biotite is produced during weathering of rocks with copper sulfide mineralization, such as porphyry copper systems.

Electron microprobe analyses of reacted micas show that phlogopite becomes more enriched in copper than biotite but that both phlogopite and biotite become enriched in silica relative to all other cations. A combination of transmission electron microscopy (TEM) observations and electron microprobe analyses indicates that copper is absorbed into the interlayer region of the micas where it exchanges for potassium. We propose that octahedrally coordinated ferrous iron reduces absorbed copper ions to metallic copper. It appears that biotite retains potassium more tenaciously than phlogopite. Higher fluorine concentrations in biotite relative to phlogopite may stabilize potassium in biotite relative to phlogopite. This, in turn, could explain why phlogopite appears to absorb copper more readily than biotite.

The results of these experiments indicate that biotite may absorb copper during in situ and heap leach mining, which could result in lowered recoveries. This is relevant to research on in situ leach mining by the U. S. Bureau of Mines, Advanced Mining Division. Biotite in mine tailings and in other types of mine workings could also act as a copper sink, which would lower copper concentrations in acidic mine drainage from some mining regions.

Introduction

ILTON and Veblen (1988) used transmission electron microscopy (TEM) and analytical electron microscopy to demonstrate that anomalous copper concentrations in biotites and chlorites from the Koluola Igneous Complex, Solomon Islands (host to a porphyry copper deposit), and from rocks associated with porphyry copper deposits at the Globe Miami district, Arizona, could be accounted for by submicroscopic inclusions of native copper. The copper inclusions lie in the interlayer regions of the sheet silicates. The inclusions are disc shaped and often exhibit polygonal morphologies when viewed parallel to c* of the enclosing mica (c* is the direction perpendicular to the basal layering). The inclusions range from 2 to 100 nm in thickness and are up to about 1,000 nm in diameter. Further, the copper inclusions are strongly associated with expanded interlayers.

Ilton and Veblen (1990, 1992) generalized the observations of Ilton and Veblen (1988) by reporting similar observations from four other intrusions associated with porphyry copper environments. At the time, Ilton and Veblen (1988) could not determine whether the copper inclusions in biotite formed during weathering or during the magmatic hydrothermal event. Ilton and Veblen (1990, 1992) provided strong evidence to support the suggestion that copper is introduced into biotite and subsequently reduced to the metallic state during supergene (or weathering) processes.

Determining the timing of copper enrichment in biotite is important because geologists have tried, for over 25 yrs, to develop the copper contents of bio-

0361-0128/92/1394/1813-17$3.00

tites into an exploration tool and into a guide for understanding magmatic hydrothermal ore-forming processes in porphyry copper systems (e.g., Parry and Nockowski, 1963; Putnam and Burnham, 1963; Lovering, 1969, 1972; Lovering et al., 1970; Graybeal, 1973; Banks, 1974; Kesler et al., 1975; Hendry et al., 1981, 1985). Determining the mode of copper enrichment in biotite at low temperatures and pressures is critical to understanding the conditions under which biotite might (1) adversely affect copper recoveries during solution mining (Cook, 1987), (2) affect the release or retention of copper during acid mine drainage, and (3) affect the supergene enrichment of copper.

This paper presents results from experiments designed, in part, to test the hypothesis put forward by Ilton and Veblen (1990, 1992) that native copper inclusions in biotite can form during the weathering of rocks with porphyry copper-style mineralization. Although the primary purpose of this paper is to compare the mode of copper enrichment in the experimental micas to that in natural micas from porphyry copper deposits, we present initial results on mica dissolution. Our experimental approach involved a combination of techniques. In order to simulate the weathering environment associated with porphyry copper deposits, we reacted biotite and phlogopite with acidic, copper sulfate-bearing aqueous fluids under low-temperature and low-pressure conditions. The U. S. Bureau of Mines has determined that similar conditions are encountered during in situ and heap leach mining (Earley, 1992). We analyzed the mica run products with the electron microprobe in order to determine the concentrations of absorbed copper and the chemical consequences of dissolution. We used X-ray mapping to show the distribution of copper in the run products and transmission electron microscopy to discern the mode of and the reactions responsible for copper enrichment in the mica run products. We have devoted a small section of the paper to aqueous speciation modeling in order to determine the saturation state of our experimental solutions with respect to copper minerals.

Experimental Methods

Starting materials

Large books of biotite from the Bancroft mine, Ontario (referred to in tables as BANBI), Canada, and phlogopite from the Comet mine, Quebec, Canada (referred to in tables as COMPHLO), were cut with a diamond gem saw into >4 mesh but $\leq 1 \times 1 \times 0.1$ cm flakes. The flakes were rinsed rapidly with deionized water. Cutting the biotite books inevitably introduces surface heterogeneities such as parted interlayers. This could, in part, account for the heterogeneous distribution of copper described in the "Results" section. We note, however, that natural biotites also display a heterogeneous distribution of copper. The starting material was analyzed and checked for homogeneity, absence of copper inclusions, and copper concentrations using electron microprobe analysis, wet chemical analysis, and transmission and analytical electron microscopy. The average unreacted mica compositions are given in Table 1. Comparison with TEM observations and electron microprobe analyses of unreacted and reacted micas, prepared in identical fashion, indicate that the features described for reacted micas were formed during the experiments and not during preparation.

The solutions were prepared by adding measured amounts of reagent grade $CuSO_4$ (Baker, lot 40715) and H_2SO_4 (Mallinckrodt, lot 5557 KXCK) to ultrapure water. The ionic strength and pH were buffered by the large fluid/rock ratio and high copper sulfate concentrations.

TABLE 1. Average Chemical Compositions of Unreacted Micas

	BANBI		COMPHLO	
	Microprobe	Wet chemistry	Microprobe	Wet chemistry
SiO_2	39.1	39.0	41.1	39.8
Al_2O_3	10.6	11.9	13.8	13.4
FeO_{total}	19.8	19.0	3.0	1.7
MgO	13.6	13.4	25.0	23.9
TiO_2	1.9	2.6	0.7	0.4
MnO	0.9	0.9	0.03	0.08
Li_2O	NA	0.2	NA	ND
CaO	0.01	0.4	ND	ND
Na_2O	0.5	0.4	0.3	ND
K_2O	9.2	8.8	10.3	9.6
SO_3	0.03	ND	0.01	ND
F	2.3	2.4	1.8	NA
Cl	0.04	<0.1	0.04	NA
Total	98	99	96	89
Cu		53 (ppm)		24 (ppm)
	Structural formulas (22 O)			
Si	5.98	5.8	5.78	5.9
Al	1.91	2.1	2.28	1.3
Fe	2.53		0.36	
Fe^{+2}		1.9		0.15
Fe^{+3}		0.47		0.06
Mg	3.11	3.0	5.24	5.3
Ti	0.22	0.29	0.08	0.05
Mn	0.12	0.1	0.004	0.01
Li	ND	0.9	NA	ND
Na	0.14	0.1	0.07	ND
K	1.8	1.7	1.86	1.8

See "Experimental Methods" section in the text for detailed information about analytical conditions, techniques, and associated errors; in wt percent unless noted otherwise

Abbreviations: BANBI = biotite from the Bancroft mine, Ontario; COMPHLO = phlogopite from the Comet mine, Quebec; NA = not analyzed; ND = not detected

Experimental design

The experiments were performed at 25° ± 3°C and 1 atm; solutions were open to the atmosphere but dissolved oxygen was not monitored. The experimental conditions are summarized in Table 2. Two types of flow through reactors were used. The first experiment (CuBi1) was performed in a short column reactor. This design is a simplified version of the one used by Knauss and Wolery (1986). A peristaltic pump circulated the solution from a polyethylene reagent tank to the reactor (Cole-Parmer Teflon filter holder) via tygon tubes. The solution entered the top of the reactor and flowed over mica flakes supported by thick Teflon filters. The solution exited the bottom of the column reactor and was collected in a polyethylene bottle for analysis. The solid products were sampled periodically for electron microprobe and transmission electron microscopy analysis.

Subsequent experiments were performed in a mixed-flow reactor. Rimstidt and Dove (1986) discuss the advantages of this design. The solution was pumped from a polyethylene bottle into the reactor (a 120-ml polyethylene bottle). A magnetic stir bar at the bottom of the reactor continuously mixed the solution. Perforated polyethylene bottles, containing the mica flakes, were positioned inside the reactor just above the stir bar. The solution was continuously pumped from the bottom of the reactor, via tygon tubing, into a sample bottle for chemical analysis.

Sample preparation for electron microprobe and transmission and analytical electron microscopy analysis

To avoid precipitation of copper on the exposed surfaces of the mica flakes during drying, the micas were extracted and immediately and rapidly rinsed at room temperature, first with a dilute HCl solution and then with ultrapure water. It is possible that the rinsing procedure might have extracted some small quantity of potassium from the interlayers or altered the exposed surfaces of the run products. However, we believe the effect would be miniscule relative to the amount of alteration that occurred during the experiments (i.e., the micas were sitting in acidic solutions for 1–3 mo). Moreover, we studied the interior portions of mica, not the exposed surfaces. Initially, we dried some mica flakes in an oven for 2 to 3 h at 50°C and some at room temperature. TEM images showed that there were no observable differences between samples dried at 50°C and at room temperatures. Subsequently, we found it expedient to dry samples at 50°C. We note that 50°C represents a hot day in the deserts of the southwest of the United States, which is home to many porphyry copper deposits.

The run products were prepared for electron microprobe and TEM analysis in two different manners. For analysis with the electron beam normal to c*, the mica flakes were treated with a silane bonding agent and then embedded in a ceramic amalgam (3M Concise) composed of quartz and a small amount of acrylic. The silane forms a more durable bond with the ceramic than the mica cleavage surface does alone. The ceramic blocks were cut with a diamond gem saw, such that the mica was bisected parallel to c*. One face of the ceramic mica billet was prepared by grinding on glass with alumina grits and then mounted face down on a glass slide with a thermoplastic cement (Aremco Crystalbond 509). Most of the billet was cut off with a diamond thin section saw. The section was thinned to approximately 100 to 200 μm with a diamond-embedded silicon-carbide grinding wheel and then thinned and polished to 30 μm with alumina grits on glass and felt, respectively. Best results were obtained when the 100-μm-thick section was released by heating and then flipped over. Immersing the specimen in ice water during grinding also helped to maintain the integrity of the embedded mica flake. If these precautions were not adhered to, the mica usually plucked out of the ceramic

TABLE 2. Experimental Parameters

Experiment no.	Solid	Starting mass (g)	$CuSO_4$ (wt %) (initial = final)	pH (initial = final)	Flow rate (ml/hr)	Time (h)
CuBi1	BANBI	0.504	12.0	3	0.594	336
CuBi2	BANBI	1.080	2.4	3.8	0.066	[1]
CuBi3						
4/12/90	BANBI	1.556	2.4	2.6	0.085	670
7/09/90	BANBI	1.556	2.4	2.6	0.085	2,806
CuBi4						
5/11/90	COMPHLO	2.719	2.4	2.6	0.068	696
6/11/90	COMPHLO	2.719	2.4	2.6	0.068	1,440
CuBi6	BANBI	2.48	2.4	3.85	0.072	792

[1] Electrode leaked KCl

Si, Al, Fe, Mg, and K < 1 ppm in outflow solution; volume of solution in reaction bottles = 120 ml

Abbreviations as in Table 1

amalgam during grinding. The section was now ready for optical, SEM, and electron microprobe analysis, but additional steps were required for TEM analysis.

For TEM analysis with the electron beam normal to c*, silver grids (o.d. 2.3 mm; i.d. 1 mm; 0.1 mm thick) were epoxied to specimens that previously had been prepared for electron microprobe analysis as described above. The grids were removed from the glass slides, and the specimens were argon-ion milled to the thickness required for electron transparency. These specimens were lightly coated with amorphous carbon to render them conductive in the electron beam. Observations were made at the thin edges of these ion-milled biotites that occur around perforations in the section.

For TEM observations on biotite with the electron beam normal to the structural layers (parallel to c*), an alternative preparation method was used. Cleaved sheets of the mica were placed between two pieces of cellophane tape and pulled apart. This process was repeated until the cleavage fragments were electron transparent (less than 0.1 μm thick). Silver grids were then epoxied to the mica sheets. After curing, the tape was pulled off with a final layer of biotite, leaving a thin layer of uncontaminated biotite on the grid.

We prepared nonreacted mica samples in the same manner as the reacted mica flakes. Electron microprobe and transmission and analytical electron microscopy analyses of these blanks suggested that our preparation techniques did not introduce measurable copper contamination.

Transmission electron microscopy

Electron microscopy was performed (at Johns Hopkins Univ.) with a Philips 420ST transmission electron microscope operated at 120 keV. A detailed description of the instrument and experimental methods is given by Veblen and Bish (1988) and Livi and Veblen (1987). Identification, orientation, and chemical information on the various phases present in the experimental run products was determined using conventional and high-resolution imaging modes, selected area electron diffraction, convergent beam electron diffraction, and X-ray emission analytical electron microscopy. The line resolution of the instrument is 0.14 nm. Electron diffraction studies of the experimentally produced copper inclusions in biotite were limited to convergent beam electron diffraction because of their extremely small size (convergent beam electron diffraction resolution is about 2 nm). Analytical resolution (90% column) varies as a function of specimen geometry and material analyzed but is a minimum of approximately 20 nm under ideal circumstances. Inclusions even smaller than 20 nm can be characterized chemically by collection of diluted spectra, followed by subtraction of the matrix analysis. X-ray spectra were collected with an EDAX lithium-drifted, solid-state, energy-dispersive detector inclined 20° to the horizontal. The detector signal was processed with a Princeton Gamma-Tech System 4 X-ray analyzer. The samples were analyzed in beryllium cup, low-background, double-tilt specimen holders at tilts between 10° and 25° toward the detector, giving effective takeoff angles between 30° and 45°. Analyses were obtained in conventional TEM mode, with spot sizes ranging from approximately 20 to 100 nm in diameter. Details concerning quantitative analysis are given in Livi and Veblen (1987). The accuracy of our analyses for most major elements is estimated to be on the order of 5 percent relative to the amount present. For Na and K, errors may be higher due to alkali loss from the analysis spot and to relatively poor sensitivity of the Si-Li detector for Na. The detection limits for most elements are 0.1 to 0.2 wt percent. Most important for this study, we estimate the detection limit for copper to be approximately 0.1 wt percent (1,000 ppm).

Electron microprobe analyses

Wavelength dispersive X-ray chemical analyses of the starting materials and reaction products were done on a JEOL 733 electron microprobe at the U. S. Bureau of Mines Twin Cities Research Center. The operating conditions for all analyses were 15 keV, 10 ($\pm$ 0.03) nA, and a beam diameter of 1 μm. Copper and sulfur Kα lines were detected by spectrometers equipped with Xe proportional detectors and LiF and PET crystals, respectively. Standard counting statistics (counts were collected until the standard deviation was $\pm$ 0.5% relative) were used for major elements, but the peaks and backgrounds for Cu and S were analyzed for 300 s. The estimated detection limits for Cu and S under these conditions are 200 and 100 ppm, respectively. Simple, well-characterized oxides and silicates were used for standards (Si quartz; Ti rutile; Al corundum; Mn metal; Fe hematite; Mg,Ca diopside, Na albite; K orthoclase; Cu cuprite; S celestite). We used the data reduction program CITZAF (Armstrong, 1989). Unreacted flakes of BANBI and COMPHLO, which were previously characterized by wet chemical and electron microprobe analysis, were analyzed alongside reacted samples to check the precision and accuracy of the analyses with respect to major elements.

Wet chemical analysis of fluids and solids

The chemical compositions of both fluids and solids were analyzed by a combination of graphite furnace AA spectroscopy, ICP emission spectroscopy, ion chromatography, and wet titration.

Micas were powdered in an agate ball mill and fused with an $LiBO_2$ flux at 950°C in a graphite crucible. The molten glass bead was quenched and dis-

solved in an HCl citric acid solution. The Li content of the micas was determined by AAS after dissolving the mica powder with an HCl-HF solution in a Teflon pressure vessel heated in a microwave oven. The ICP analyses were matrix matched using synthetic standards and were checked against external standards: NBS 2704, USGS W2, USGS DNC-1, and Swedish Slag 6. The accuracies of all the ICP analyses were at least 5 percent. The AA analyses were checked against external standards only, and the accuracy obtained for Na and K is 5 percent; for Li, Cu, and Zn the reported accuracy is 15 percent.

Fe^{+2} in mica was determined by wet titration. The samples were decomposed by HCl and HF and then completely digested and titrated with potassium dichromate. Barium diphenylamine sulfonate was used as a titration point indicator. $NaCO_3$ was added to the sample solution to prevent oxidation. The estimated accuracy of this method is 5 percent.

Cl and F in the micas were measured by ion chromatography. The mica powders were fused with $LiBO_2$, and the glass beads were dissolved in a nitric acid solution. The uncertainty of the F analyses determined by this method is about 25 percent due to loss of F, possibly through formation of SiF_4 gas during some runs. The accuracies of the Cl analyses are also about 25 percent because of low Cl concentrations in these micas.

Results

Aqueous ion modeling

Aqueous speciation and copper mineral saturation states were computed for the fluids with the U. S. G. S. computer program WATEQ4F. The thermodynamic data base of Nordstrom et al. (1989) was used.

Speciation calculations suggest that the free or hydrated copper complex ($Cu^{+2} \cdot nH_2O$) and the copper sulfate complex are the predominant copper species in all the experimental solutions. In the 12 wt percent solution, 27 percent of the total copper is present as Cu^{+2} and 73 percent as $CuSO_4^0$. In the 2.4 wt percent solution, at pH = 2.6, 50 percent of the total copper is present as Cu^{+2} and 50 percent is present as $CuSO_4^0$. In the 2.4 wt percent solution, at pH = 3.8, 49 percent of the total copper is present as Cu^{+2}, and 51 percent is present as $CuSO_4^0$.

Calculations indicate that the bulk solution in CuBi1 (12 wt percent $CuSO_4$) was supersaturated with respect to chalcanthite but that the bulk solutions in CuBi3 and CuBi4 (2.4 wt percent $CuSO_4$) were undersaturated with respect to all known copper minerals. No visible precipitation occurred in the bulk solution of any of the experiments. A copper sulfate mineral, however, did precipitate on the surface of biotites from CuBi1 during the experiment.

Optical and SEM microscopy

Optical and SEM examination of the experimental run products revealed only subtle changes in the microscopic properties of the minerals during the course of the experiments. A blue copper sulfate mineral, perhaps chalcanthite (see "Aqueous ion modeling"), precipitated on the edge of and between partially cleaved layers of the biotite grains during experiment CuBi1. No precipitation was detected during any other experiment. Reacted biotites were noticeably darker than unreacted biotites when viewed by transmitted light, possibly because of partial oxidation of octahedral iron or absorption of light by submicroscopic copper inclusions. SEM observations indicate some degradation and rounding of edges in the biotite and phlogopite reaction products. Light microscopy of phlogopite shows some weakening of absorption and birefringence at the grain boundaries.

Electron microprobe analyses

In general, biotite and phlogopite absorbed appreciable concentrations of copper, but not sulfur. Representative microprobe analyses of reacted micas are listed in Tables 3 and 4. A high percentage of microprobe analyses from near the edges of crystals have low totals. This is probably caused by variable degrees of hydration and by the difficulty in avoiding holes because the micas are more frayed near the grain boundaries. We measured up to 1.2 wt percent copper as CuO, with no detectable sulfur, in CuBi1. Figure 1 is a copper X-ray map of CuBi1. Little or no sulfur is associated with copper that has migrated more than about 10 μ into biotite. Note that the high copper intensities closely follow the folds in the biotite, which is consistent with copper absorption along the interlayer sites. Biotites reacted in solutions at pH = 3.8 (CuBi6) absorbed much less copper than in solutions at lower pH.

We will focus the remainder of this section on experiments CuBi3 and CuBi4. Biotite and phlogopite contain up to 1 to 4 wt percent copper (as CuO), with no detectable sulfur. One exception is analysis 39 in Table 4. Figure 2a and b shows that copper concentrations are highest within 50 to 100 μm of the grain edge but that high copper density also is found in narrow layers that have penetrated deeper into the crystal (up to 250 μm). In general, these anomalous layers contain the highest copper concentrations.

Copper absorption profiles of biotite and phlogopite normal to c^* are illustrated in Figures 3 and 4, respectively. The large variation in the copper concentrations at a given distance from the grain edges is caused, in large part, by the heterogeneous distribution of copper that was described previously (Figs. 1 and 2). After one month of reaction, biotite and phlo-

TABLE 3. Representative Electron Microprobe Analyses of Sample CuBi3 4/12/90 (BANBI reacted for 1 mo in 2.4 wt % $CuSO_4$ solution)

Analysis no.	34	11	21	14	27	32
d (μ)	35	5	23	54	45	107
SiO_2	34.1	31.6	38.3	40.1	38.6	37.2
TiO_2	1.9	1.8	2.3	2.3	2.3	2.2
Al_2O_3	9.0	8.7	11.1	10.7	10.9	13.9
MnO	0.75	0.72	0.82	0.90	0.79	0.78
FeO	15.0	13.9	17.9	18.0	18.0	17.3
MgO	11.3	11.1	13.8	14.2	13.7	13.5
CaO	0.13	0.03	0.09	0.06	n.d.	n.d.
Na_2O	0.51	0.57	0.60	0.63	0.63	0.66
K_2O	6.7	7.2	8.6	9.0	9.3	8.7
CuO	0.92	0.40	0.30	0.12	0.053	n.d.
SO_3	n.d.	n.d.	n.d.	n.d.	n.d.	n.d.
Total	80.3	76.0	93.9	95.9	94.2	94.3
Atomic proportions						
Si	6.12	6.02	5.92	6.04	5.95	5.69
Ti	0.26	0.26	0.27	0.26	0.27	0.25
Al	1.9	2.0	2.0	1.9	2.0	2.5
Mn	0.11	0.12	0.11	0.12	0.10	0.10
Fe	2.26	2.22	2.32	2.27	2.33	2.20
Mg	3.02	3.15	3.18	3.20	3.15	3.10
Ca	0.03	0.01	0.02	0.01	n.d.	n.d.
Na	0.18	0.21	0.18	0.19	0.19	0.20
K	1.5	1.7	1.7	1.7	1.8	1.7
Cu	0.13	0.057	0.035	0.014	0.006	n.d.
Total	15.5	15.7	15.7	15.7	15.8	15.8

Abbreviations: BANBI = biotite from the Bancroft mine, Ontario; d (μ) indicates the distance perpendicular to the edge of the crystal; n.d. = below detection limit

Atomic proportions were calculated assuming a total anion charge of 44; see "Experimental Methods" section in the text for detailed information about analytical conditions, techniques, and associated errors

gopite average 0.4 and 0.8 wt percent copper (as Cu) near the crystal edge, respectively. After one month of reaction, copper concentrations in biotite and phlogopite decrease to near the detection limit at 60 to 80 and at 150 to 200 μm from the grain boundary, respectively (Figs. 3a and 4a). Comparison of absorption profiles for biotite (Fig. 3a and b) indicates that after nearly four months of reaction biotite has not absorbed appreciably more copper. In fact, it appears that biotite starts to lose copper near the edge. This might be a manifestation of dissolution with concomitant degradation of the biotite structure and loss of copper. The effects of dissolution are discussed later. A comparison of the one- and two-month phlogopite experiments (Fig. 4a and 4b) indicates that the depth of copper penetration nearly doubles from one to two months. It appears that phlogopite continues to absorb copper for at least up to two months of reaction.

After two months of reaction, electron microprobe analyses of phlogopites reveal a significant negative correlation between copper and potassium concentration; copper concentration rises linearly with decreasing potassium, whereas the data indicate near independence between copper and Si, Al, Fe, Mg, and Ti concentrations (Fig. 5 and Table 5). One-month experiments yielded similar results. Ternary and higher order covariance tests, however, were not applied. This is consistent with the work of Cook (1988) on natural biotites from the oxidized portion of the Cyprus Casa Grande porphyry copper deposit and suggests that a Cu-K exchange reaction might be operative.

The data indicate no significant correlations between copper and cation concentrations in biotite after one month of reaction (Fig. 6 and Table 5). Four-month experiments yielded similar results. Although copper and potassium are poorly correlated

TABLE 4. Representative Electron Microprobe Analyses of Sample CuBi4 6/11/90 (COMPHLO reacted for 2 mo in 2.4 wt % $CuSO_4$ solution)

Analysis no.	39	12	26	23	32	36
d (μ)	50	8	28	54	160	477
SiO_2	39.0	39.6	40.3	40.8	39.3	39.8
TiO_2	1.2	1.3	1.3	1.3	1.2	1.3
Al_2O_3	12.3	13.0	13.3	14.0	14.1	14.1
MnO	0.08	0.03	0.08	0.03	n.d.	0.05
FeO	2.0	2.1	2.0	2.0	1.9	2.1
MgO	23.8	23.7	24.0	25.5	26.0	25.8
CaO	0.27	0.28	0.19	0.05	0.07	n.d.
Na_2O	0.16	0.19	0.18	0.20	0.18	0.20
K_2O	5.8	8.2	8.8	9.8	10.6	10.7
CuO	4.4	2.4	1.1	0.63	0.24	0.013
SO_3	0.03	n.d.	n.d.	n.d.	n.d.	n.d.
Total	89.0	90.7	91.1	94.3	93.7	94.0
Atomic proportions						
Si	5.87	5.86	5.90	5.80	5.65	5.69
Ti	0.14	0.14	0.14	0.14	0.13	0.14
Al	2.18	2.26	2.29	2.34	2.39	2.38
Mn	0.01	0.004	0.01	0.004	n.d.	0.006
Fe	0.25	0.25	0.24	0.24	0.23	0.25
Mg	5.34	5.23	5.24	5.40	5.57	5.51
Ca	0.044	0.045	0.031	0.008	0.01	n.d.
Na	0.048	0.053	0.051	0.056	0.050	0.056
K	1.1	1.6	1.6	1.8	2.0	2.0
Cu	0.50	0.27	0.12	0.068	0.026	0.002
S	0.003	n.d.	n.d.	n.d.	n.d.	n.d.
Total	15.5	15.7	15.7	15.8	16.0	16.0

Abbreviations: COMPHLO = phlogopite from the Comet mine, Quebec; d (μ) indicates the distance perpendicular to the edge of the crystal; n.d. = below detection limit

Atomic proportions were calculated assuming a total anion charge of 44; see "Experimental Methods" section in the text for detailed information about analytical conditions, techniques, and associated errors

FIG. 1. Cu Kα X-ray map superimposed on an SEM image of CuBi1. The high density of copper X-rays at the very edge of the crystal is due to a copper sulfate precipitate. None of the copper X-rays issuing from the crystal interior are associated with sulfur or any other element.

in biotite relative to phlogopite (Table 5), the bulk of the low potassium analyses in biotite occur at the higher copper values in biotite. Copper concentrations tend to plateau at ~0.04 atoms per-formula-unit with decreasing potassium. Apparently, potassium loss becomes decoupled from copper absorption at higher copper concentrations.

Microprobe data yield initial results on mica dissolution in acidic copper sulfate solutions. Figures 7 and 8 show that biotite and phlogopite are becoming enriched in silica relative to all other cations; dissolution of both phlogopite and biotite produced a silica-enriched fringe. Earley et al. (1990) also observed silica enrichment in reaction products of biotites from core leaching experiments. A comparison of the slopes of the regression equations in Figures 7 and 8 (see Table 5) indicate that cations other than Si (and K in phlogopite) appear to dissolve more closely to their stoichiometric proportions, where the degree of enrichments in the reacted micas are (Fe, Mg, Al, Ti) > K and (Fe, K, Mg, Al, Ti) > Na for phlogopite and biotite, respectively. The relative loss of potassium from phlogopite is even more accentuated in the one-month experiments. Further experimental data, from fluid analyses as well as solid analyses, and statistical analyses will be required to determine the level of confidence associated with and the generality of these enrichment trends. The important point, however, is that potassium seems to be retained more tenaciously by biotite than phlogopite.

At least two competing reactions were operative during the experiments; copper absorption by and dissolution of the micas. In this regard, note that much of the variance in the copper versus cation plots is associated with high silica concentrations (see Figs. 5 and 6). In particular, dissolution might have

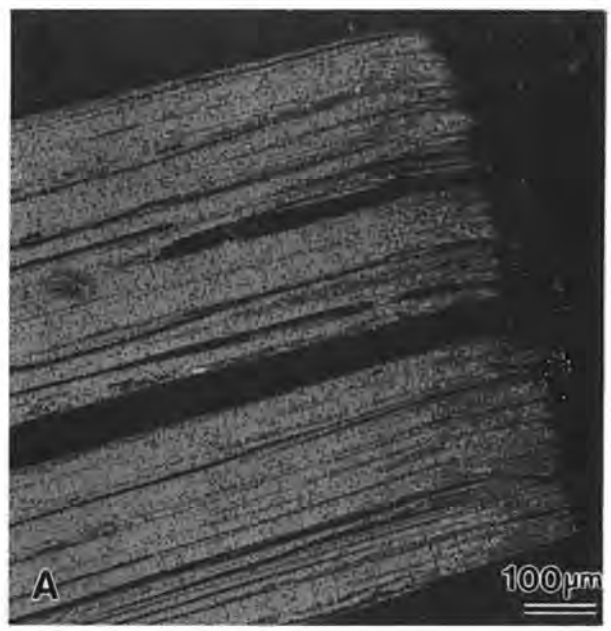

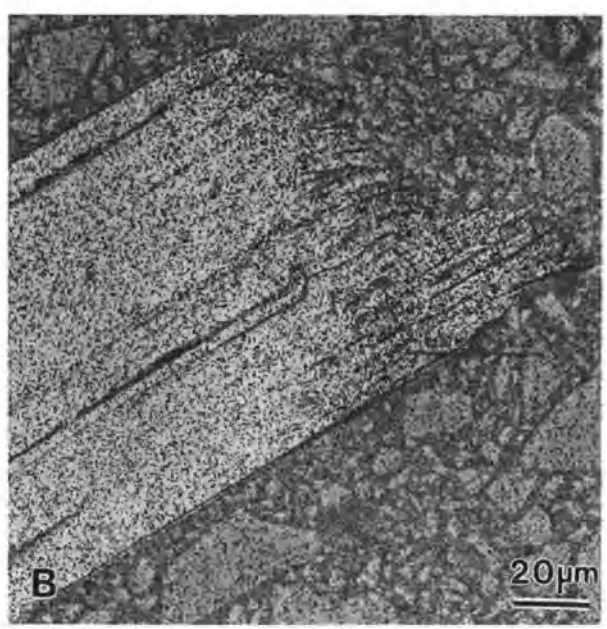

FIG. 2. Cu Kα X-ray maps superimposed on SEM images of (A) CuBi4 5/11/90 and (B) CuBi3 7/9/90. None of the copper X-rays issuing from the crystal interior are associated with sulfur or any other element.

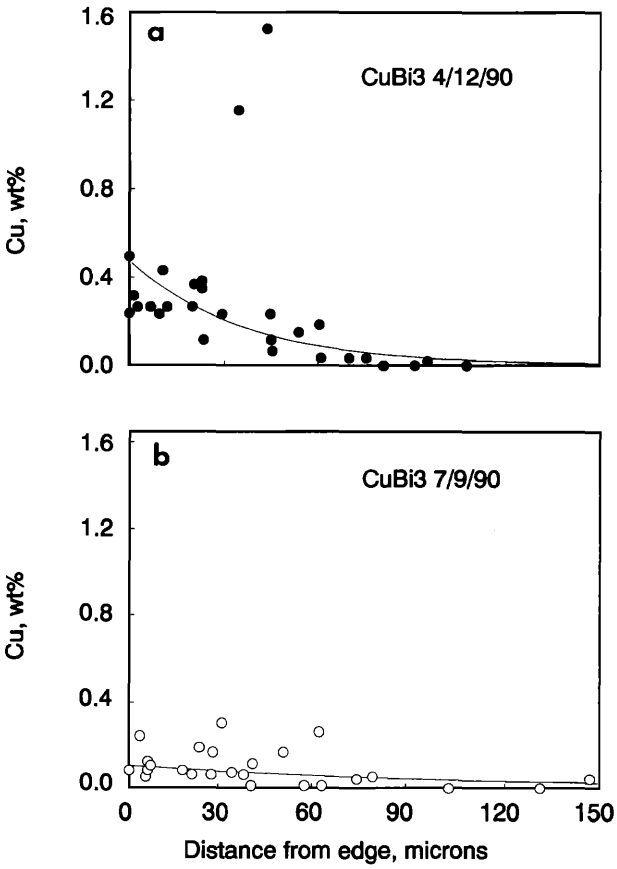

FIG. 3. Copper absorption profiles perpendicular to c° for (a) CuBi3 4/12/90 and (b) CuBi3 7/9/90. Concentration of copper in biotite is plotted against distance from the edge of the crystal.

obscured evidence for a Cu-K exchange in biotite (see Fig. 6), whereas the Cu-K exchange has affected the Si-K regression for phlogopite. A more rigorous statistical treatment of the data, however, is beyond the scope of this paper.

Phlogopite continued to absorb copper from one to two months (Fig. 4). Presumably, continued dissolution and increasing diffusional path lengths for potassium would eventually either establish a steady state copper absorption profile in phlogopite or reverse the process, as appears to have happened for biotite after four months of reaction (Fig. 3).

One should note that the correlation coefficients for the copper cation regressions, listed in Table 5, were calculated assuming nonclosure. Obviously, this is a false assumption because the compositional data are constrained by a fixed sum. The closure constraint, however, becomes less severe with increasing numbers of components (10 in our case) and, perhaps more importantly, we can attribute a physical significance to the correlation coefficients based on TEM observations and the bonding environment of potassium in biotite relative to phlogopite, as discussed below. We did not calculate correlation coefficients for silica cation regressions because the interpretation of this data is relatively simple (i.e., silica enrichment with dissolution).

Transmission electron microscopy

Submicroscopic inclusions of a high copper, sulfur-absent phase in both phlogopite and biotite (CuBi1, CuBi3, and CuBi4) were produced in as little as 13 to 30 days. The inclusions are disk shaped when viewed parallel to c° of the enclosing mica (Fig. 9), with diameters up to 20 nm, occasionally twinned (Fig. 9b), and located within and associated with expanded interlayers (Figs. 10 and 11). Comparison of unreacted and reacted biotites demonstrates that copper enrichment and inclusion formation are associated with hydrated biotite interlayers, as indicated

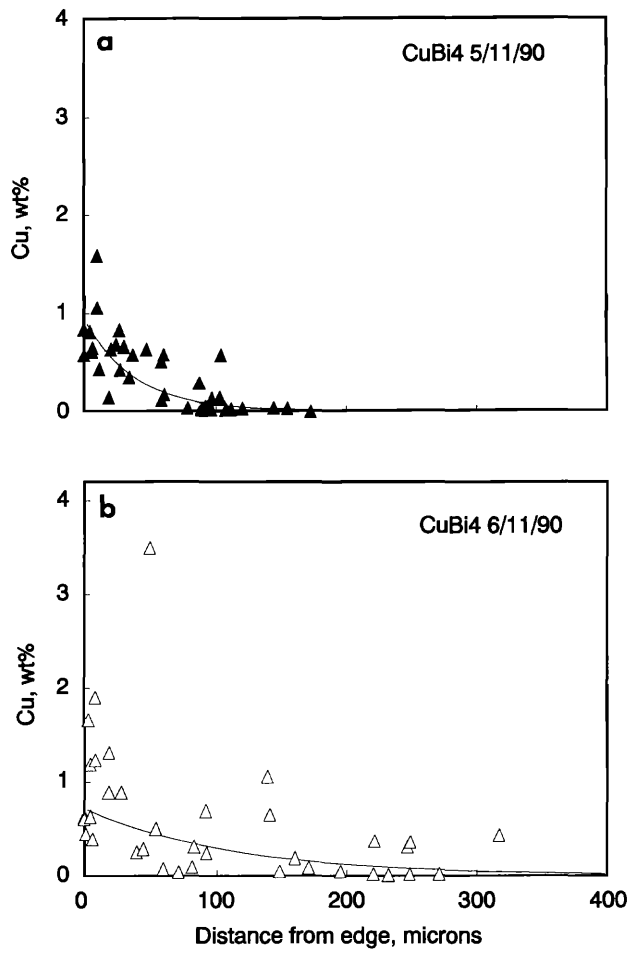

FIG. 4. Copper absorption profiles perpendicular to c° for (a) CuBi4 5/11/90 and (b) CuBi4 6/11/90. Concentration of copper in biotite is plotted against distance from the edge of the crystal.

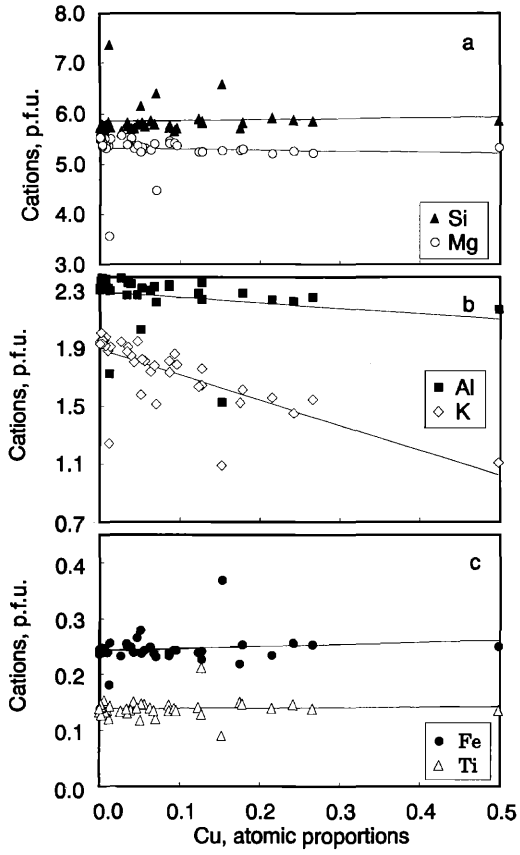

FIG. 5. (a) Si and Mg, (b) Al and K, and (c) Fe and Ti concentrations plotted versus the concentrations of copper in phlogopite (CuBi4 6/11/90). p.f.u. = per formula unit.

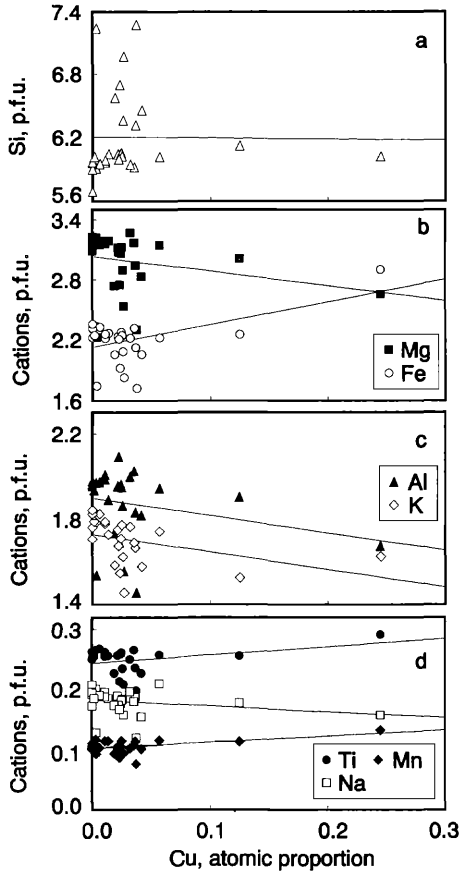

FIG. 6. (a) Si, (b) Mg and Fe, (c) Al and K, and (d) Ti, Mn, and Na concentrations plotted versus copper concentrations in biotite (CuBi3 4/12/90). p.f.u. = per formula unit.

by more prominent light fringes in high-resolution TEM images, similar to those reported previously from naturally weathered biotites (Banfield and Eggleton, 1988). Analytical electron microscopy of the inclusions reveals only copper, although elements with atomic numbers less than 11 are not measur-

TABLE 5. Slopes, Intercepts, and Correlations for Figures 5, 6, 7, and 8

Figures	5 (phlogopite)			6 (biotite)				7 (biotite)		8 (phlogopite)	
	Slope	Intercept	r	Slope	Intercept	r		Slope	Intercept	Slope	Intercept
Cu/Si	0.20	5.85	0.06	−0.10	6.20	−0.01	Si/Al	−0.42	4.50	−0.50	5.21
Cu/Mg	−0.19	5.32	−0.05	−1.48	3.04	−0.26	Si/Fe	−0.44	4.95	−0.02	0.27
Cu/Al	−0.38	2.30	−0.22	−0.82	1.90	−0.25	Si/Mg	−0.63	6.91	−0.98	11.1
Cu/K	−1.74	1.89	−0.73	−0.82	1.73	−0.41	Si/K	−0.31	3.59	−0.51	4.75
Cu/Fe	0.04	0.24	0.15	2.26	2.13	0.49	Si/Ti	−0.05	0.56	−0.02	0.27
Cu/Ti	0.01	0.14	0.05	0.14	0.24	0.30	Si/Mn	−0.02	0.22		
Cu/Na				−0.09	0.18	−0.23	Si/Na	−0.04	0.44		
Cu/Mn				0.10	0.10	0.45					

Data fit to the linear equation $y = mx + b$, where {cations} = m{Cu} + b and {cations} = m {Si} + b for Figures 5 and 6, and Figures 7 and 6, respectively; correlation coefficients (r) are given only for copper cation regressions (see text); the correlation coefficients were calculated assuming nonclosure; this is a false assumption and, although the closure constraint becomes less severe with increasing numbers of components (10 in our case), the r values given here should have a tendency to be negatively biased (Aitchison, 1986); for Figure 5, $P < 0.001$ and $P > 0.1$ for r values associated with Cu/K, and Cu/Si, Al, Mg, Fe, and Ti, respectively; for Figure 6, $0.05 > P > 0.01$ and $P > 0.1$ for r values associated with Cu/K, Fe, and Mn, and Cu/Si, Al, Mg, Ti, and Na, respectively

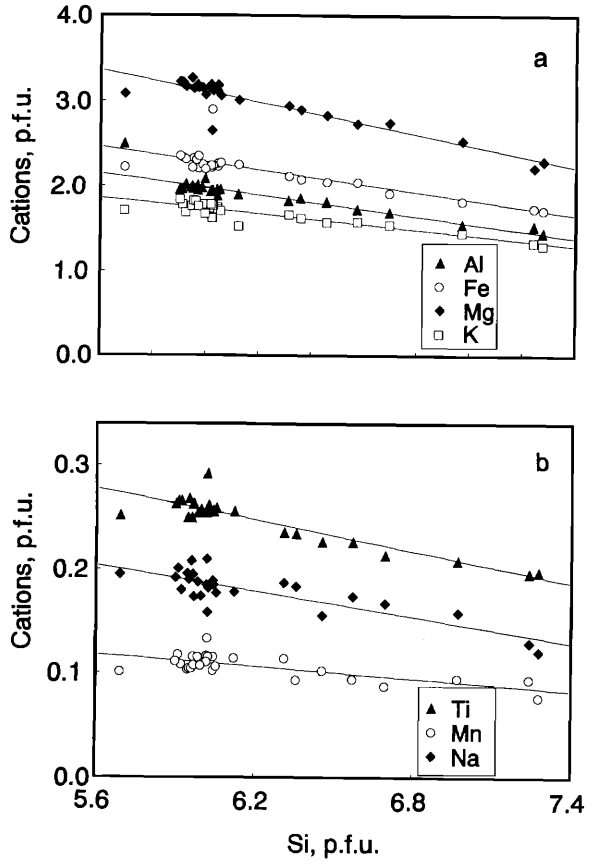

FIG. 7. (a) Mg, Fe, Al, and K, and (b) Ti, Mn, and Na concentrations plotted versus silica concentrations in biotite (CuBi3 4/12/90). p.f.u. = per formula unit.

able. Analytical electron microscopy analyses together with electron diffraction data (Fig. 12), however, are consistent with the identification of the inclusions as native copper.

Mica alteration can be described by an edge weathering model (Fanning and Keramidas, 1977). The absorption fronts are associated with potassium depletion, expanded interlayers, submicroscopic native copper inclusions, and copper enrichment up to 1 to 4 wt percent (reported as CuO). Areas showing the highest copper enrichment in phlogopite and biotite contain a high density of copper inclusions and copper-enriched expanded interlayers distributed along narrow lenticular zones (tens to hundreds of nanometers thick) that are parallel to the basal cleavage. Analytical electron microscopy demonstrates that areas without expanded interlayers or copper inclusions do not contain detectable copper (i.e., they contain <1,000 ppm Cu). In the phlogopite experiments, domains with expanded interlayers but no copper inclusions are shown by analytical electronmicroscopy to contain up to 0.3 (±0.1) wt percent copper as CuO (Fig. 13), whereas in the biotite experiments measurable copper is restricted to areas with copper inclusions. An SEM image (Fig. 2a) of phlogopite shows a copper sorption front with narrow copper-rich zones (or zippers) that penetrate phlogopite past the front. Presumably, copper-rich zippers at the electron microprobe scale correspond to areas rich in copper inclusions and copper-enriched expanded interlayers. The development of these zippers might be controlled by defects. Alternatively, zippers may originate at surface heterogeneities, which may or may not have been introduced during preparation. TEM studies of both reacted and unreacted biotites and phlogopites have not resolved this issue thus far. Similar heterogeneous distributions of copper, however, are observed in natural biotites (Ilton and Veblen, 1988).

High-resolution TEM of reacted micas has not revealed any precipitates, other than native copper, in

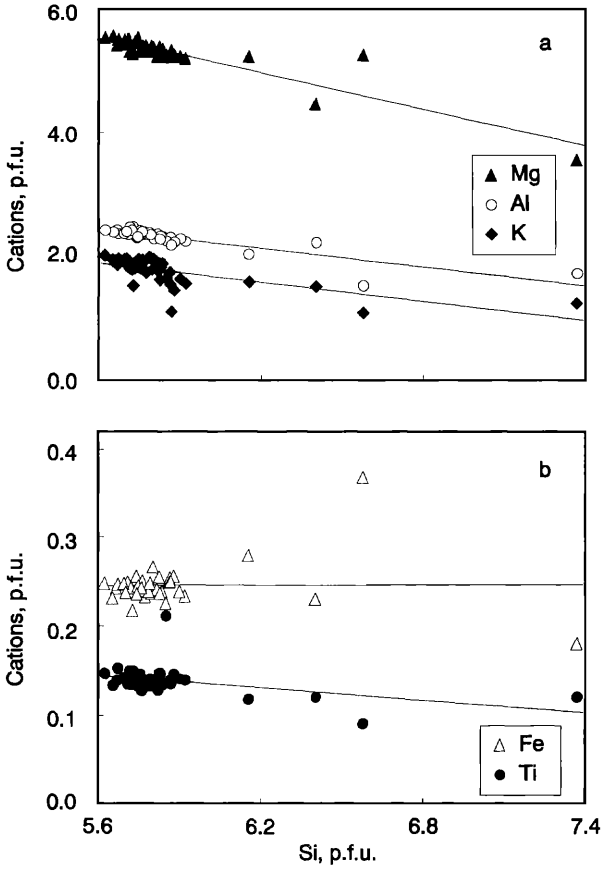

FIG. 8. (a) Mg, Al, and K, and (b) Ti and Fe concentrations plotted versus silica concentrations in phlogopite (CuBi4 6/11/90). p.f.u. = per formula unit.

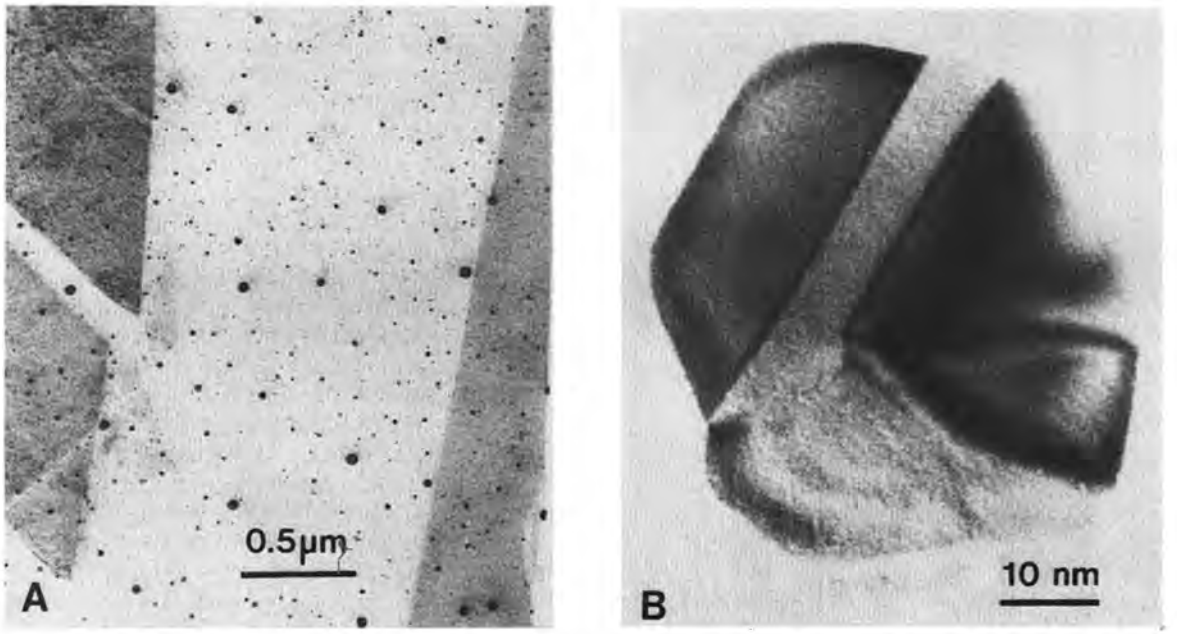

FIG. 9. TEM photomicrographs of CuBi1, after 336 h of reaction, viewed normal to the layers. Note that this biotite layer was in the interior portion of the mica during the experiment and was not an exposed surface. A. Numerous dark inclusions are metallic copper. B. Enlarged view of an inclusion from Figure A. Note that the inclusion is twinned, as in natural samples. The pseudohexagonal morphology of the inclusion was probably inherited from the biotite substrate.

the interlayer region. Because of the nature of the technique, however, we have not surveyed a large volume of biotite. More work is required to determine the generality of these observations. We plan to use high-resolution SEM (15 Å resolution) to help survey exposed sheets and mica edges.

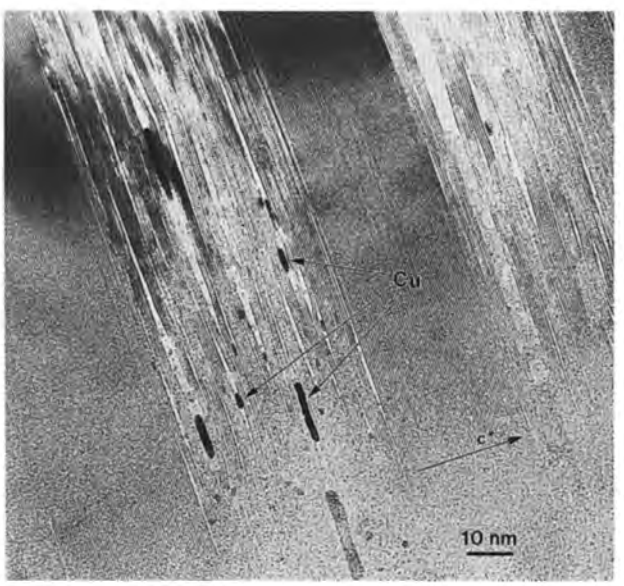

FIG. 10. TEM photomicrograph of biotite CuBi1, after 336 h of reaction, viewed parallel to the layers. The dark inclusions lying within the interlayers are metallic copper. Note the close association of the inclusions with expanded interlayers.

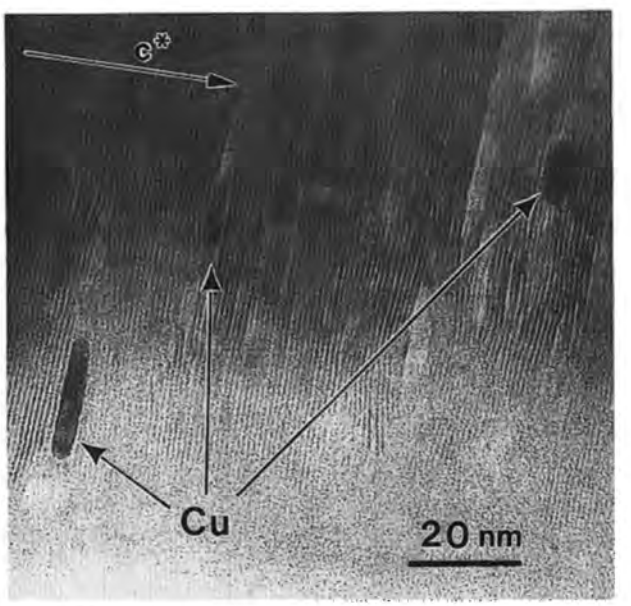

FIG. 11. TEM photomicrograph of phlogopite CuBi4 6/12/90, viewed parallel to the layers. The dark inclusions lying within the interlayers are metallic copper.

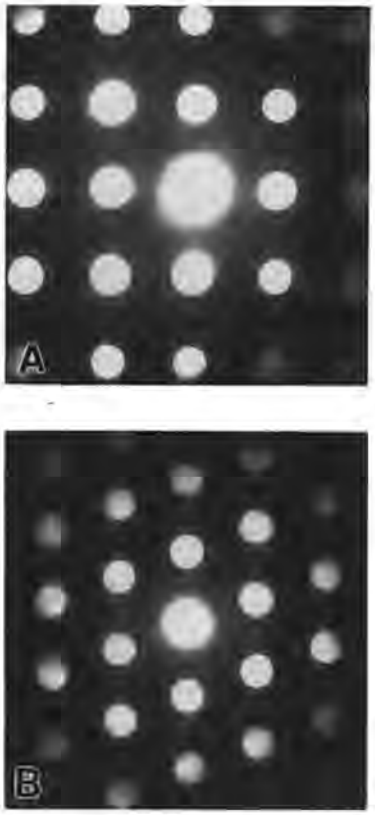

FIG. 12. Convergent beam electron diffraction patterns from a copper inclusion. (A) [001] zone axis and (B) [011] zone axis of metallic copper. The electron diffraction patterns were formed by focusing a condensed electron beam on the inclusions. See "Transmission electron microscopy" section in the text for details.

Discussion

Comparison of the experimental observations and conditions to natural systems

The mode of copper enrichment in biotite and phlogopite and the associated alteration textures produced by the experiments are very similar to those found in samples of copper-enriched biotites from porphyry copper environments, as described by Ilton and Veblen (1988, 1990, 1992). Similarities between experimental and naturally occurring copper-enriched biotites include the presence of hydrated, potassium-depleted alteration domains that contain copper-enriched expanded interlayers and submicroscopic native copper inclusions. In addition, some natural samples have domains with minor copper enrichment associated with expanded interlayers and no copper inclusions, similar to such zones produced in the phlogopite experiments. In both the experimental and natural samples, copper inclusions are commonly located within expanded interlayers. One difference between the natural and experimental biotites is that some of the natural inclusions are larger than those produced in our experiments.

The experiments support the contention of Ilton and Veblen (1990) that the formation of copper inclusions in biotite and copper enrichment of biotites can occur during weathering of mineralized rocks associated with porphyry copper deposits. This is consistent with the electron microprobe study of Rehrig and McKinney (1976). The solutions used in these experiments have copper and sulfate concentrations at the upper range of those found in porphyry copper deposit mine waters but lower concentrations of aluminum, iron, and potassium (each cation < 1 ppm) than those reported for mine waters (see Table 6). The experimental solutions lie in the more acidic region given by Sato (1960) as typical of solutions produced by sulfide weathering and have pH values similar to those calculated by Ague and Brimhall (1989) for the weathering of main-stage mineralization at Butte, Montana. Differences between the compositions of the experimental solutions and fluid compositions produced by weathering of porphyry copper mineralization may influence the amount and mode of copper absorption by biotite. Ilton and Veblen (1990, 1992) have documented that the mode of copper enrichment in natural biotites is complex and varies with depth in the oxidized zone. In particular, copper-rich biotites do not necessarily contain native copper inclusions. A wider range of fluid compositions and physical conditions must be explored in order to account for different modes of copper incorporation in naturally occurring biotites.

Reactions associated with copper absorption

TEM observations and microprobe analyses of the experimental run products indicate that copper inclusion formation is intimately associated with interlayer hydration and potassium depletion in the mica and that copper is introduced along the interlayers in exchange for K^+. In particular, the negative correlation between copper and potassium in phlogopite (Fig. 5) is consistent with the TEM observation that copper enrichment is associated with expanded in-

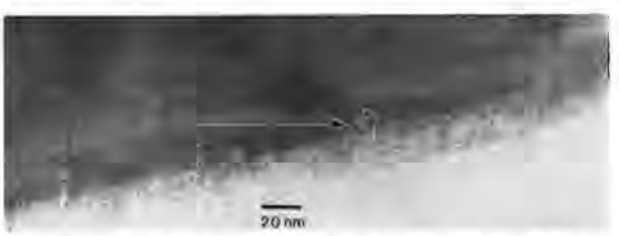

FIG. 13. TEM photomicrograph of phlogopite CuBi4 6/12/90, viewed parallel to the layers. Note the presence of expanded interlayers without copper inclusions. Analytical electron microscopy showed this area to contain detectable copper (a few thousand ppm).

TABLE 6. Water Analyses from Copper Sulfide Mines (in ppm)

Sample	pH	Mg	SO_4	Cu	Al	SiO_2	Ca	Fe	K	Na	Alkali
1	3.2	300	13,683	5,220	397	144	461	891	9	100	
2	3.0	1,415	17,493	886	1,670	146	541	104	1	28	
3	3.7	1,383	15,557	12	260	139	542	843	2	28	
4	6.7	117	1,296		31	55	481		6	53	
5		149	71,053	45,633	85	67	307				48
6		62	2,672	59	84	48	133				52
7		41	6,664	312	433	56	68				42
8		63	2,068	41	165	79	238				13
9		61	5,064	1,659		76	436				
10		36	1,419		16	28	319				170
11		86	4,457	60	22	56	753				198
12		82	3,898	122	44	40	239				97
13		54	1,335	28	9	20	277				14
14		165	29,325	718	1,550	44	194				38

Analyses 1 to 4 from the Silver Bell mine (Marozas, 1982); analyses 5 to 14 given by Emmons (1917): 5 = Mountain View mine, Butte, Montana; 6 = St. Lawrence mine, Butte, Montana; 7 = Burra Burra mine, Ducktown, Tennessee; 8 = East Tennessee mine, Ducktown, Tennessee; 9 to 13 = Capote mine, Cananea, Mexico; 14 = Mineral Park mine, Kingman, Arizona (seep at the base of tailings)

terlayers. Electron microprobe data for reacted phlogopite indicate that the exchange of Cu^{+2} for K^+ is nearly 1:2 (Table 5). Whereas the overall Cu-K exchange reaction is close to 1:2, it is not clear whether hydration of the interlayers occurs first ($H_3O^+ \rightarrow K^+$), followed by exchange of copper ions in solution for interlayer H_3O^+, or whether there is a direct exchange of copper ions for interlayer potassium ions. This is an important question given that Newman (1970) demonstrated that H^+ had a synergistic effect on the exchange of Na^+ for K^+ in micas. Indeed, initial results indicate that pH might influence copper absorption by biotite, where copper absorption by biotite might be enhanced at lower pH (e.g., CuBi3 vs. CuBi6). Other experimental parameters between CuBi3 and CuBi6, however, were not identical.

At present, we cannot explain satisfactorily the poor correlation between potassium and copper in the biotite experiments (Fig. 6). As discussed above, it is possible that biotite might favor a $H_3O^+ \rightarrow K^+$ exchange relative to a $Cu^{+2} \rightarrow K^+$ exchange.

High-resolution TEM images of the reacted micas indicate that copper is not forming brucite-like sheets (i.e., copper chlorites) in the interlayers such as those described in XRD studies of naturally occurring hydroxy Cu vermiculites by Basset (1958) and Ildefonse et al. (1986) (i.e., we have not imaged the brucite-like layer). The most likely alternative is that copper-enriched expanded interlayers in the reacted micas are filled by differing stoichiometries of K^+, H_3O^+, and variably hydrated Cu^{+2}.

Copper is reduced and precipitated in biotite in the form of submicroscopic native copper inclusions. The only known reductant in our experiments is ferrous iron in biotite. We suggest, therefore, that octahedrally coordinated ferrous iron in biotite reduces interlayer copper ions to native copper. Moreover, initial results from Mössbauer spectroscopy indicate that appreciable iron oxidation has occurred in reacted biotite (Darby Dyar, pers. commun.). Studies by Sayin et al. (1979), White and Yee (1985), and Eary and Rai (1989) have shown that Fe^{+2}-bearing silicates are potentially strong reductants of multivalent cations in solution. Other work suggests that interlayer copper can catalyze the oxidation of Fe^{+2} in sheet silicates (Rozenson and Heller-Kellai, 1976; Sayin, 1982). The phlogopite experiments were implemented to define the minimum concentration of octahedrally coordinated ferrous iron in biotite needed to reduce interlayer copper ions to the metal. The results of the phlogopite experiments, however, are ambiguous, because of the presence of 2.1 wt percent FeO in the phlogopite and the formation of copper inclusions. Experiments using phlogopites with only 0.2 wt percent FeO are now in progress.

In summary, based on evidence from these experiments, we suggest that native copper inclusions in natural biotites were formed by the following reactions:

$$Cu^{+2}_{aq} + 2K^{+}_{\text{interlayered}} = K^{+}_{aq} + Cu^{+2}_{\text{interlayered}} \quad (1)$$

and

$$Cu^{+2}_{\text{interlayered}} + 2Fe^{+2}_{\text{octahedral}} = Cu^{o}_{\text{interlayered}} + 2Fe^{+3}_{\text{octahedral}}. \quad (2)$$

The details of the electron transfer mechanism, however, are not understood.

Comparison of the biotite and phlogopite experiments

A strict comparison of the phlogopite and biotite experiments is not possible at this time because of

differences in experimental parameters between the two sets of experiments (Table 2). The fact that phlogopite profiles (Fig. 4), however, are more enriched in copper than biotite profiles (Fig. 3) is consistent with what we would predict based on differences in the fluorine contents of the two micas. Higher fluorine and dioctahedral component in micas tend to retard the release of potassium to solution (see review by Fanning and Keramidas, 1977). In fact, Hoda and Hood (1972) showed that fluorine is the strongest determinant of potassium stability in micas during weathering. The compositions of the unreacted micas show that biotite contains 38 mole percent more fluorine that phlogopite, whereas neither biotite nor phlogopite have an appreciable dioctahedral component (Table 1). Consequently, we would expect biotite to retain its potassium more tenaciously than phlogopite. This, in turn, would allow phlogopite to absorb copper more readily than biotite. Indeed, the compositional data (see "Results") indicate that potassium was more stable in biotite relative to phlogopite. Note that this occurs despite the fact that the fluid flow rates and solution/mica mass ratios were higher in the biotite experiments (CuBi3) than in the phlogopite experiments (CuBi4).

Another factor that influences the stability of potassium in micas is the oxidation of octahedral iron (see reviews by Fanning and Keramidas, 1977; and Scott and Amonette, 1988). Although the effect of iron oxidation on the behavior of interlayer potassium is not thoroughly understood, the consensus is that initial oxidation of iron promotes the release of potassium to solutions by reducing layer charge; continuing oxidation is accompanied by expulsion of octahedral iron, which increases the dioctahedral nature of the mica and stabilizes interlayer potassium (Scott and Amonette, 1988). Obviously, these factors would influence biotite more than phlogopite. The experiments, however, were not constrained to elucidate the influence of iron oxidation on interlayer potassium stability.

Comparison of Figure 6a and c shows that the high variance of the copper-potassium data for biotite is associated with high silica concentrations; Figure 6c shows that potassium concentrations appear to become independent of copper concentrations at $\sim$0.04 per formula unit copper. In contrast, the correlation of potassium and copper is much stronger for phlogopite than biotite (see Table 5). Given two competing reactions, copper absorption and dissolution, we suggest that potassium loss from biotite, relative to phlogopite, is coupled more strongly to dissolution; whereas potassium depletion in phlogopite, relative to biotite, appears to be associated more strongly with copper absorption. An explanation for this apparent difference in behavior between biotite and phlogopite requires more work, but such a difference might be related to the bonding environment of potassium in biotite relative to phlogopite, as discussed above.

Comparison of our experiments to other work on the dissolution of micas

Comparison of our experiments with other work on the dissolution of micas is compromised by differences in experimental parameters and design. Despite these differences, some of our results are similar to previous work. In particular, micas from other dissolution studies also became silica enriched (e.g., Gastuche, 1963; Gilkes et al., 1973; Lin and Clemency, 1981a and b). Lin and Clemency (1981a) showed that phlogopite (2 wt percent F) dissolved incongruently in a closed system, where the enrichment trend in phlogopite was Si > Mg > K. This compares well with our results for phlogopite. Lin and Clemency (1981a) determined the dissolution behavior of phlogopite from fluid analyses and could not determine the behavior of Al and Fe because these elements precipitated. Clemency and Lin (1981) showed that phlogopite dissolved congruently, after the first hour of reaction, in an open system (they used a resin to absorb dissolved cations). Although we maintained an open system, flow rates were relatively slow. Experiments at higher flow rates might yield congruent dissolution.

A number of experiments on the dissolution of micas have been performed with organic chelating agents (see review by Scott and Amonette, 1988). Organic acids can be strongly cation selective and as such could dictate the mode of mica dissolution. It is beyond the scope of this paper to compare our results with such work.

Relevance to leach and heap mining operations

The experiments are relevant to the U. S. Bureau of Mines efforts to develop in situ leach mining technology for porphyry copper deposits (U. S. Bur. Mines IC 9216, 1989). Our findings are also applicable to heap leach mining operations and to environmental problems related to acid mine drainage. The experiments show that the sorption rate of copper by biotite and phlogopite is relevant to the lifetime of an in situ mining operation. Moreover, the dominant mode of copper incorporation in biotite and in other silicates might dictate the most efficient chemistries for the leach solutions. The injected solutions of in situ leach mining operations are more acidic than the solutions used in this study. Uptake of copper by biotite may be limited at pH < 2, because the 2/1 layers of the mica structure are attacked vigorously, and sorbed copper is released as the structure degrades (Earley et al., 1990). However, pH values in the range of 2 to 4 have been measured in evolved solutions from recycled core-leaching experiments on copper oxide ores (S. Paulson, pers. commun.) and

from the Cyprus Casa Grande in situ leach mining operation (Earley, 1992). An important question is whether recycled leach solutions will build up enough potassium to inhibit copper uptake by biotite, or will conditioning of the deposit be necessary in order to avoid "preg-robbing" (i.e., robbing the "pregnant" solution of its metal value) by biotite? The same question applies to heap leaching operations, although the solution chemistries can be controlled more easily in this type of system.

Future work

A kinetic study of copper absorption by and dissolution of biotite is in progress. The results should be particularly useful in modeling copper transport during weathering of porphyry copper deposits with high biotite and feldspar concentrations, minimum sericitization and argillic alteration, and relatively low pyrite/chalcopyrite ratios. Under these conditions, acid production is limited, the acid buffering capacity is maximized, and biotite may be preserved for the length of active supergene processes. The Cyprus Casa Grande deposit (formerly Lakeshore) in Arizona is an example of such a deposit (Cook, 1988; Huyck, 1990). At the Cyprus Casa Grande deposit, biotite in the goethite zone contains from 20 to 60 percent of the whole-rock copper (Cook, 1988). Submicroscopic inclusions of native copper account for a considerable proportion of the copper in biotites from the goethite zone (Ilton and Veblen, 1990, 1992).

Because our TEM observations and microprobe analyses indicate that copper ions are absorbed along the interlayers of biotite and phlogopite, it is reasonable to suggest that the kinetics and absolute amount of copper absorption by biotite will be strongly affected by the bonding environment of potassium in mica and by the relative concentrations of potassium and exchangeable cations in solution. Factors that affect the cation exchange of potassium in biotite are reviewed by Fanning and Keramidas (1977) and Scott and Amonette (1988). For example, Rausell-Colom et al. (1965) and Hoda and Hood (1972) showed that fluorine in micas tends to retard the release of potassium to aqueous solution. This, in turn, might affect copper absorption by biotite. The fluorine contents of the biotite and phlogopite used in our experiments were considerably higher than those of biotites typically associated with porphyry copper deposits. Therefore, one of our priorities will be to perform experiments with low fluorine biotites.

Other important experimental parameters that require further investigation include temperature and solution composition. It would be particularly important to perform experiments with a wide range of potassium concentrations and pH values. Experiments at elevated temperatures would be necessary to determine if the copper inclusions are truly diagnostic of weathering regimes.

Conclusions

We reacted biotite and phlogopite with acidic copper sulfate solutions at 25° ± 3°C and 1 atm. Electron microprobe analyses indicate that the micas absorbed appreciable copper within one month of reaction. TEM observations and electron microprobe analyses suggest that copper substitutes for potassium in the micas and that appreciable copper also occurs as submicroscopic native copper inclusions in the interlayer region of the micas. The mode of copper enrichment in the experimental micas, such as submicroscopic native copper inclusions and copper-enriched expanded interlayers, is similar to that reported by Ilton and Veblen (1990, 1992) for biotites from weathered portions of the Cyprus Casa Grande porphyry copper deposit, Arizona. The experiments support the hypothesis that biotite can become enriched in copper and that native copper inclusions can precipitate in biotite during the weathering of rocks with porphyry copper-style mineralization. The experiments provide evidence that octahedrally coordinated ferrous iron in biotite is the reducing agent for copper.

Electron microprobe analyses of reacted phlogopite and biotite indicate that silica enrichment of both phlogopite and biotite occurred during dissolution. The data also indicate that biotite retained potassium more tenaciously than phlogopite and that phlogopite is more copper enriched than biotite. Higher fluorine concentrations in biotite relative to phlogopite may explain this apparent difference in the reactivity of the two micas.

This study demonstrates the utility of electron microprobe techniques and high-resolution TEM for characterizing micas from dissolution experiments and for examining in detail the reactions responsible for copper absorption by some trioctahedral micas. We suggest that high-resolution TEM should be routinely applied to absorption studies. Such detailed observations are necessary for better understanding the reaction mechanisms and conditions responsible for metal attenuation by or metal mobilization from solid phases in the near-surface environment.

Acknowledgments

This research was funded in part by DOE contract DE-FGO2-89ER 14074, awarded to D. R. V. and E. S. I. Electron microscopy was performed at the Johns Hopkins high-resolution TEM-analytical electron microscopy lab, which was established with partial support from National Science Foundation grant EAR 83-00365. We thank James Webster, Ted Eary, James Sjoberg, and two *Economic Geology* reviewers for thoughtful critiques of the manuscript. Support

by the DOE for this work does not constitute an endorsement by the DOE of the views expressed in this article.

June 4, 1991; April 7, 1992

REFERENCES

Ague, J. J., and Brimhall, G. H, 1989, Geochemical modeling of steady state fluid flow and chemical reaction during supergene enrichment of porphyry copper deposits: ECON. GEOL., v. 84, p. 506–528.

Aitchison, J., 1986, The statistical analysis of compositional data: New York, NY, Chapman Hall, 416 p.

Armstrong, J. T., 1989, CITZAF: A microprobe/SEM correction program, version 3.03: Pasadena, California Inst. Technology.

Banfield, J. F., and Eggleton, R. A., 1988, Transmission electron microscope study of biotite weathering: Clays and Clay Minerals, v. 36, p. 47–60.

Banks, N. G., 1974, Distribution of copper in biotite and biotite alteration products in intrusive rocks near two Arizona porphyry copper deposits: U. S. Geol. Survey Jour. Research, v. 2, p. 195–211.

Basset, W. A., 1958, Copper vermiculites from northern Rhodesia: Am. Mineralogist, v. 43, p. 1112–1133.

Clemency, C. V., and Lin, F.-C., 1981, Dissolution kinetics of phlogopites. II. Open system using an ion-exchange resin: Clays and Clay Minerals, v. 29, p. 107–112.

Cook, S. S., 1987, Petrologic analysis of laboratory core leaching experiments, *in* Coyne, K. R., and Hiskey, J. B., eds., In situ recovery of minerals: New York, Engineering Foundation, p. 81–98.

—— 1988, Supergene copper mineralization at the Lakeshore mine, Pinal County, Arizona: ECON. GEOL., v. 83, p. 297–309.

Earley, D., III and Jones, P. M., 1992, Geochemical effects on the hydrology of in-situ leach mining of copper oxide ore at the Cyprus Casa Grande mine, Arizona: Soc. Mining Engineers Ann. Mtg., Pheonix, Arizona, Feb. 24–27, 1992, SME/AIME Preprint 92-242, 10 p.

Earley, D., III, Paulson, S. E., and Brink, S. E., 1990, The effects of rock mineralogy, chemistry, and texture on in situ leaching of oxide copper ores from the Santa Cruz deposit, Arizona: Soc. Mining Engineers Ann. Mtg., Salt Lake City, Utah, Feb. 26–March 1, 1990, SME/AIME Preprint 90-182, 8 p.

Eary, L. E., and Rai, D., 1989, Kinetics of chromate reduction by ferrous ions derived from hematite and biotite at 25°C: Am. Jour. Sci., v. 289, p. 180–213.

Emmons, W. H., 1917, The enrichment of ore deposits: U. S. Geol. Survey Bull. 625, 530 p.

Fanning, D. S., and Keramidas, V. Z., 1977, Micas, *in* Dixon, J. B., and Weed, S. B., eds., Minerals in soil environments: Madison, Wisconsin, Soil Sci. Soc. America, p. 195–241.

Gastuche, M. C., 1963, Kinetics of acid dissolution of biotite. I. Interfacial rate process followed by optical measurement of the white silica rim: Internat. Clay Conf., Stockholm, 1963, Proc., v. 1, p. 67–76.

Gilkes, R. J., Young, R. C., and Quirk, J. P., 1973, Artificial weathering of oxidized biotite: II. Rates of dissolution in 0.1, 0.01, 0.001 *M* HCl: Soil Sci. Soc. America Proc., v. 37, p. 29–33.

Graybeal, F. T., 1973, Copper, manganese, and zinc in coexisting mafic minerals from Laramide intrusive rocks in Arizona: ECON. GEOL., v. 68, p. 785–798.

Hendry, D. A. F., Chivas, A. R., Reed, S. J. B., and Long, J. V. P., 1981, Geochemical evidence for magmatic fluids in porphyry copper mineralization. Part II. Ion probe analysis of Cu contents of mafic minerals, Koloula igneous complex: Contr. Mineralogy Petrology, v. 78, p. 404–412.

Hendry, D. A. F., Chivas, A. R., Long, J. V. P., and Reed, S. J. B., 1985, Chemical differences between minerals from mineralizing and barren intrusions from some North American porphyry copper deposits: Contr. Mineralogy Petrology, v. 89, p. 317–329.

Hoda, S. N., and Hood, W. C., 1972, Laboratory alteration of trioctahedral micas: Clays and Clay Minerals, v. 20, p. 343–358.

Huyck, H. L. O., 1990, The Lakeshore porphyry copper deposit, Pinal County, Arizona: Geological setting and physical controls of mineralization: Canadian Mining Metall. Bull., v. 83, no. 937, p. 77–88.

Ildefonse, P., Manceau, A., Prost, D., and Groke, M. C. T., 1986, Hydroxy-Cu-vermiculite formed by the weathering of Fe-biotite at Salabo, Carajas, Brazil: Clays and Clay Minerals, v. 34, p. 338–345.

Ilton, E. S., and Veblen, D. R., 1988, Copper inclusions in sheet silicates from porphyry Cu deposits: Nature, v. 334, p. 516–518.

—— 1990, The origin and mode of copper enrichment in biotites from porphyry copper environments: A transmission electron microscopy study [abs.]: Geol. Soc. America Abstracts with Programs, v. 22, p. A360.

—— 1992, The origin and mode of copper enrichment in biotites from porphyry copper environments: A transmission electron microscopy study: ECON. GEOL.

Kesler, S. E., Issigonis, M. J., Brownlow, A. H., Damon, P. E., Moore, W. J., Northcote, K. E., and Preto, V. A., 1975, Geochemistry of biotites from mineralized and barren intrusive systems: ECON. GEOL., v. 70, p. 559–567.

Knauss, V. G., and Wolery, T. J., 1986, Dependence of albite dissolution kinetics on pH and T at 25°C and 70°C: Geochim. et Cosmochim. Acta, v. 50, p. 2481–2497.

Lin, F.-C., and Clemency, C. V., 1981a, Dissolution kinetics of phlogopite. I. Closed system: Clays and Clay Minerals, v. 29, p. 101–106.

—— 1981b, The kinetics of dissolution of muscovites at 25°C and 1 atm CO_2 partial pressure: Geochim. et Cosmochim. Acta, v. 45, p. 571–576.

Livi, K. J. T., and Veblen, D. R., 1987, "Eastonite" from Easton, Pennsylvania: A mixture of phlogopite and a new form of serpentine: Am. Mineralogist, v. 72, p. 113–125.

Lovering, T. G., 1969, Distribution of minor elements in samples of biotite from igneous rocks: U. S. Geol. Survey Prof. Paper 650-B, p. B101–B106.

—— 1972, Distribution of minor elements in biotite samples from felsic intrusive rocks as a tool for correlation: U. S. Geol. Survey Bull., v. 1314-D, 29 p.

Lovering, T. G., Cooper, J. R., Drewes, H., and Cone, G. G., 1970, Copper in biotite from igneous rocks in southern Arizona as an ore indicator: U. S. Geol. Survey Prof. Paper 700-B, p. B1–B6.

Marozas, D., 1982, The role of silicate mineral alteration in the supergene enrichment process: Unpub. M.S. thesis, Univ. Arizona, 58 p.

Newman, A. C. D., 1970, The synergetic effect of hydrogen ions on the cation exchange of potassium in micas: Clay Minerals, v. 8, p. 361–373.

Nordstrom, D. K., Plummer, L. N., Langmuir, D., Busenberg, E., May, H. M., Jones, B. F., and Parkhurst, D. L., 1989, Revised chemical equilibrium data for major water-mineral reactions and their limitations: Adv. Chemistry Ser. 416, p. 398–413.

Parry, W. T., and Nockowski, M. P., 1963, Copper, lead and zinc in biotites from basin and range quartz monzonite: ECON. GEOL., v. 58, p. 1126–1144.

Putnam, G. W., and Burnham, C. W., 1963, Trace elements in igneous rocks, northwestern and central Arizona: Geochim. et Cosmochim. Acta, v. 27, p. 53–106.

Rausell-Colom, J. A., Sweatman, T. R., Wells, C. B., and Norrish, K., 1965, Studies in the artificial weathering of micas, *in* Hallsworth, E. G., and Crawford, D. V., eds., Experimental pedology: London, Buttersworth, p. 40–72.

Rehrig, W. A., and McKinney, C. N., 1976, The distribution and

origin of anomalous copper in biotite [abs.]: Mining Engineering, v. 27, p. 68.

Rimstidt, D. J., and Dove, P. M., 1986, Mineral/solution reaction rates in a mixed flow reactor: Wollastonite hydrolysis: Geochim. et Cosmochim. Acta, v. 50, p. 2509–2516.

Rozenson, I., and Heller-Kellai, L., 1978, Reduction and oxidation of Fe^{3+} in dioctahedral smectites-III. Oxidation of octahedral iron in montmorillonites: Clays and Clay Minerals, v. 26, 88–92.

Sato, M., 1960, Oxidation of sulfide ore bodies, 1. Geochemical environments in terms of Eh and pH: ECON. GEOL., v. 55, p. 928–961.

Sayin, M., 1982, Catalytic action of copper on the oxidation of structural iron in vermiculated biotite: Clays and Clay Minerals, v. 30, p. 287–290.

Sayin, M., Beyme, B., and Graf von Reichenbach, H., 1979, Formation of metallic silver as related to iron oxidation in K-depleted micas: Internat. Clay Conf., Oxford, 1978, Proc., p. 177–186.

Scott, A. D., and Amonette, J., 1988, The role of iron in mica weathering: NATO ASI Ser. C, v. 217, p. 537–623.

U. S. Bureau of Mines, 1989, In situ leach mining: Inf. Circ. 9216, 107 p.

Veblen, D. R., and Bish, D. L., 1988, TEM and X-ray study of orthopyroxene megacrysts: Microstructures and crystal chemistry: Am. Mineralogist, v. 73, p. 677–691.

White, A. F., and Yee, A., 1985, Aqueous oxidation-reduction kinetics associated with coupled electron-cation transfer from iron-containing silicates at 25°C: Geochim. et Cosmochim. Acta, v. 49, p. 1263–1275.